Surprising new dynamics phenomena in Diels–Alder reaction of C_{60} uncovered with AI

Yi-Fan Hou, Quanhao Zhang, and Pavlo O. Dral*

State Key Laboratory of Physical Chemistry of Solid Surfaces, College of Chemistry and Chemical Engineering, Fujian Provincial Key Laboratory of Theoretical and Computational Chemistry, and Innovation Laboratory for Sciences and Technologies of Energy Materials of Fujian Province (IKKEM), Xiamen University, Xiamen, Fujian 361005, China

Email: dral@xmu.edu.cn

Abstract

Our recently developed physics-informed active learning allowed us to perform extensive AI-accelerated quasi-classical molecular dynamics investigation of the time-resolved mechanism of Diels–Alder reaction of fullerene C_{60} with 2,3-dimethyl-1,3-butadiene. In a substantial fraction (10%) of reactive trajectories, the larger C_{60} non-covalently attracts the 2,3-dimethyl-1,3-butadiene long before the barrier so that the diene undergoes the series of complex motions including roaming, somersaults, twisting, and twisting somersaults around the fullerene until it aligns itself to pass over the barrier. These complicated processes could be easily missed in typically performed quantum chemical simulations with shorter and fewer trajectories. After passing the barrier, the bonds take longer to form compared to the simplest prototypical Diels–Alder reaction of ethene with 1,3-butadiene despite high similarities in transition states and barrier widths evaluated with intrinsic reaction coordinate (IRC) calculations.

Diels–Alder reaction is paradigmatic and was extensively studied experimentally and theoretically. The textbook example is the reaction of ethene as a dienophile with 1,3-butadiene which was observed experimentally.[1, 2] The small system size allowed for detailed static quantum chemical (QC)[3-5] and quasi-classical molecular dynamics (MD)[3] simulations of this reaction that revealed the symmetric transition state (TS) structure and the preference for a concerted mechanism (Figure 1).

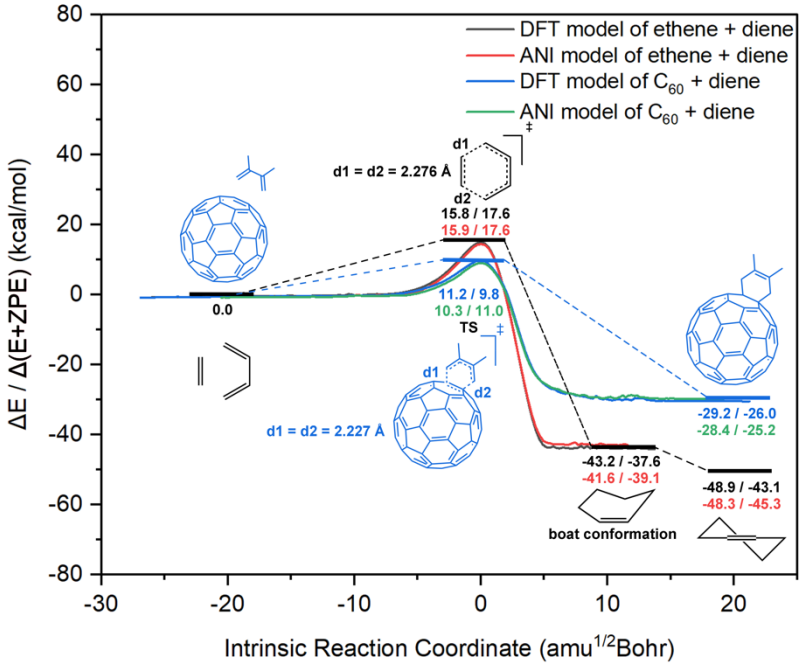

Figure 1. Energy diagram and IRC analysis of Diels–Alder reactions of 1,3-butadiene with ethene (black and red) and 2,3-dimethyl-1,3-butadiene with fullerene C_{60} (blue and green) at UB3LYP-D4/6-31G* and ANI surrogate model.

However, many chemically interesting Diels–Alder reactions involve much bigger molecules,[6-8] which may have very different behavior compared to small systems. For example, this reaction type provides a powerful route for the functionalization of fullerenes[6-8] and was used to form an adduct of fullerene C_{60} with 2,3-dimethyl-1,3-butadiene which is the main subject of this study (Figure 1). The typical fullerene size alone constitutes a challenge for QC simulations and the above system comprising fullerene and diene has 76 atoms. This imposes a big limitation on performing extensive analysis of the time-resolved mechanism of the reaction with quasi-classical MD. The MD simulations of the similarly-sized but smaller system with 57 atoms were reported to take almost 2–6 days for a single trajectory on 16 CPUs.[9] To make matters worse, such investigations require[10] many hundreds of trajectories to obtain precise results and detect rare events. Due to the cost limitations, the propagation time is also limited and the dynamics is often propagated just long enough to see the bond

formation and breaking events as defined by some cutoffs. Any interesting events occurring after this would be missed. Hence, the MD simulations of the Diels–Alder reactions with bigger molecules are very costly, require high-performance computing (HPC) facilities, and are prohibitively expensive in many cases.

Luckily, advances in artificial intelligence (AI) allow us to bring the simulation cost down and enable investigations of big systems and longer time scale.[11-13] AI has been instrumental in understanding and discovering interesting mechanistic details in chemical reactions such as roaming.[14-17] The bottleneck of such AI studies is the construction of robust machine learning potentials and many solutions based on active learning (AL) were suggested to overcome it.[18-25] For example, AL on small prototypical systems contributed to the understanding that in Diels–Alder reactions, the type of performed dynamics (NVE vs NVT or classical vs ring-polymer MD) has a small effect on the outcome.[26] One of AL solutions is also our recent efficient physics-informed AL protocol which was able to reproduce the earlier quasi-classical MD investigation[3] of the ethene and 1,3-butadiene at UB3LYP/6-31G* in a fraction of computational cost without requiring any HPC.[27]

Here, this AL protocol enabled us to investigate the time-resolved mechanism of the Diels–Alder reaction between fullerene C_{60} and 2,3-dimethyl-1,3-butadiene on a much larger scale than similar state-of-the-art QC investigations (see *Computational details*).[3] The high quality of the machine learning potential ANI our protocol produced is clearly seen by comparing to DFT static calculations of barrier heights, reaction energies, and IRC shown in Figure 1. We propagated one thousand forward and backward quasi-classical trajectories with ANI to obtain statistically precise results and extended the propagation time to 1500 fs: this is 10 times longer than in the previous study[3] on the reaction of much smaller ethene and 1,3-butadiene. More trajectories and longer simulations have allowed us to uncover phenomena previously unknown for this reaction, which smaller-scale simulations would have missed. Many studies have reported trajectories of several or dozens picoseconds.[15, 17, 28] Although it is a piece of cake for ML models to run long trajectories, we did not push the propagation that far because of the potential zero-point energy leakage.[29] The zero-point energy of high-frequency modes will flow into low-frequency modes, resulting in faster rotation and even dissociation.[29]

Our quasi-classical MD simulations showed that the large size of the C_{60} and 2,3-dimethyl-1,3-butadiene reactants leads to a dynamics behavior in rare trajectories qualitatively different from the cycloaddition reaction of ethene and 1,3-butadiene (Figure 2).

Unlike the reaction between ethene and 1,3-butadiene where two reactants move closer to each other and form bonds directly without roaming, the bulkier 2,3-dimethyl-1,3-butadiene undergoes a prolonged phase of alignment around the C_{60} buckyball in 10% of the reactive trajectories (Figure 3). During the alignment phase, the diene displays complex 'acrobatic' movements such as somersault (4.6%), twisting (3.9%), twisting somersault (1.4%), and other roaming (0.4%) (Figure 2, videos of selected trajectories are available on [url upon publication]). We assume that the alignment phase happens if the distances between two bonding carbon atoms and C_{60} are shorter than 5.0 Å after 1.5 ps; otherwise, the trajectories are deemed to correspond to a direct reaction.

All of the calculations were performed with the UB3LYP[30]-D4[31]/6-31G*[32, 33] level because B3LYP/6-31G* was shown to be a suitable and affordable method for reaction description as it provides similar results to the higher-level QC calculations.[34, 35] D4 dispersion corrections were included in the calculations as their effect is non-negligible, particularly for a large system, according to the static calculations, see Table S2 in Supporting Information (SI). In our AL procedure, we used the ANI-type model[36] as a surrogate for UB3LYP-D4/6-31G*. Predictions of ANI models in a fraction of trajectories exceeded thresholds defined by our uncertainty quantification[27] procedure; these uncertain trajectories were removed so that only confident results were analyzed.

Remarkably, dynamics simulations unveiled the substantial differences between the two reactions investigated here, which the static calculations are incapable of capturing. The static calculations show that the bonds being formed are very similar in TSs of both reactions: 2.23 Å in C_{60}+2,3-dimethyl-1,3-butadiene and 2.27 Å in ethene+1,3-butadiene, despite their very different sizes (Figure 1). Also, static intrinsic reaction coordinate[37] (IRC) calculations do not show any big difference in the barrier width (Figure 1).

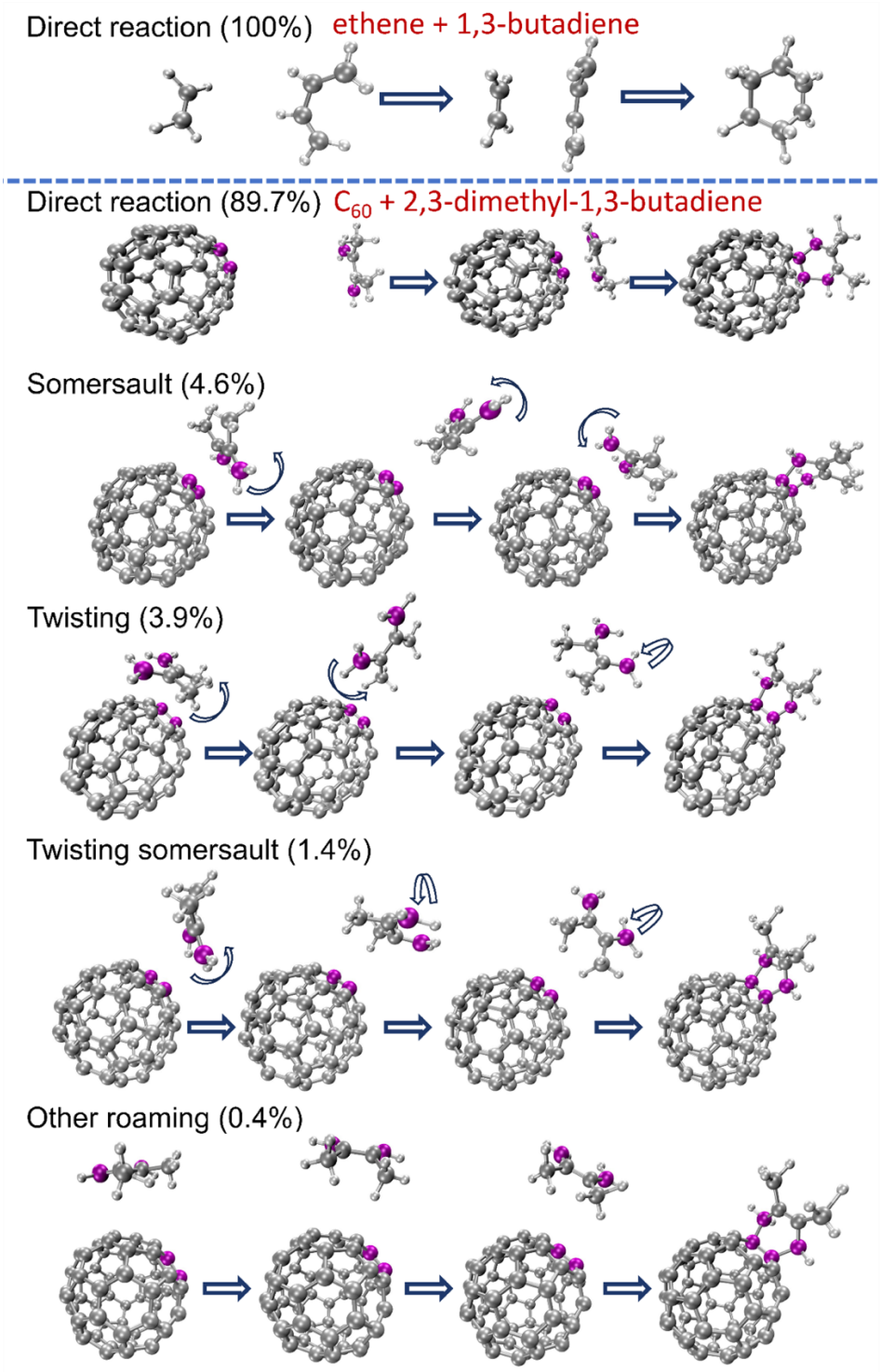

Figure 2. Snapshots of reactive trajectories of two Diels–Alder reactions. The carbon atoms of two forming C–C bonds in the reaction between 2,3-dimethyl-1,3-butadiene and fullerene are highlighted in purple. Numbers in the parenthesis are percentages of different reaction pathways to the total number of reactive trajectories. The somersault means that the diene molecule rotates around the axis along the double bond, while the twisting means the diene molecule rotates around the axis perpendicular to the molecule plane.

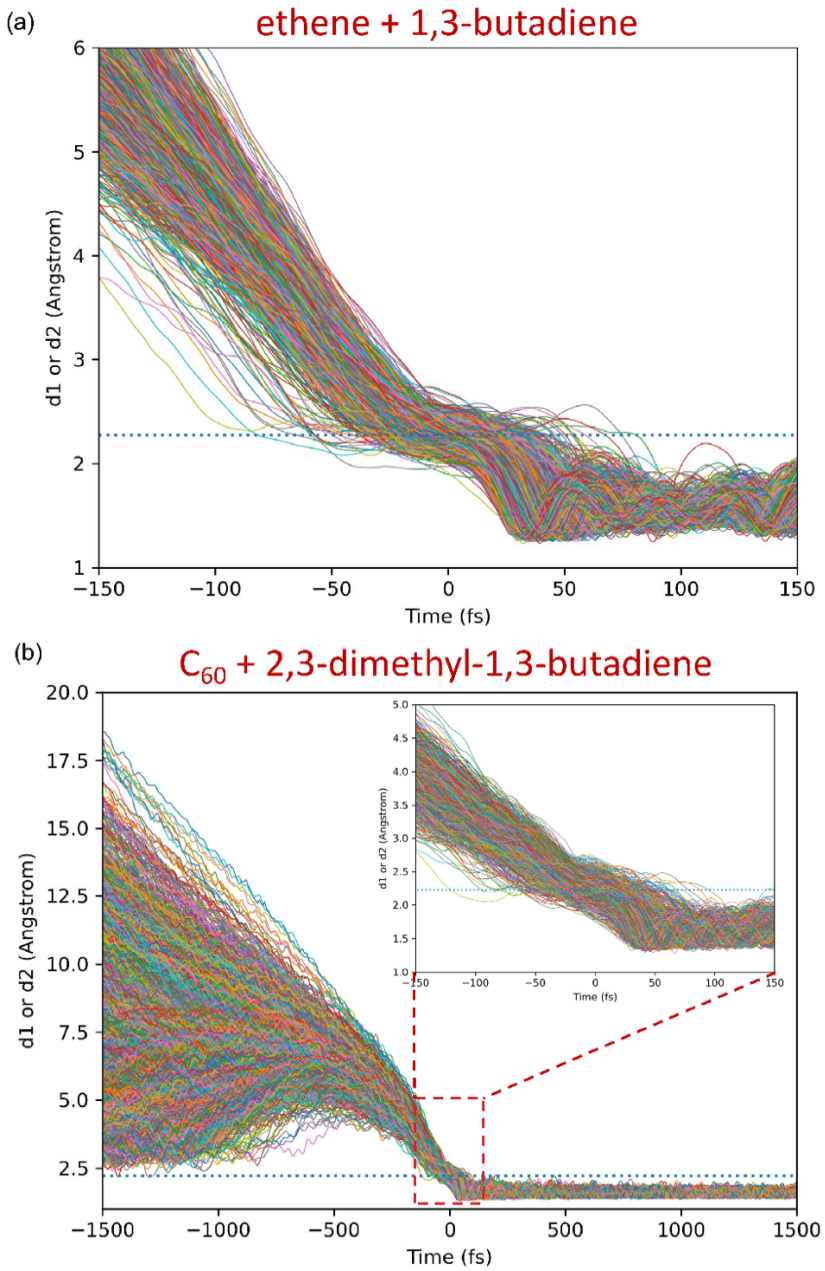

Figure 3. The C–C distance for atom pairs forming bonds as a function of time in the reactive quasi-classical MD trajectories for the Diels–Alder reaction a) between 1,3-butadiene and ethene and b) between 2,3-dimethyl-1,3-butadiene and fullerene. The blue dot lines show the distances in the TSs.

In contrast, the quasi-classical MD shows that the bond formation and dissociation in the Diels–Alder reaction of fullerene are slower than in the reaction of ethene after passing the TS (Table 1). After crossing the TSs, the bonds are broken and formed much slower in the C_{60} reaction than in the ethene reaction: 95% of the C–C bonds are formed within 88.0 fs and 69.0 fs, respectively, and 95% of the bonds are dissociated within 372.0 fs and 160.0 fs, respectively (Figure 4). Similarly, the average time of bond formation is 23% slower and the

average bond dissociation time is slower by a fraction of 2.2. In this analysis, we adopted the previous thresholds in distances: 1.6 Å and 5.0 Å for bond forming and dissociation, respectively (both bonds are considered).[3] In addition, the C_{60} and 2,3-dimethyl-1,3-butadiene find themselves 50% (30 fs) longer in the transition zone compared to the smaller system of ethene and 1,3-butadiene (Table 1 defined as the forming C–C bond length range that includes 98% of the initial points obtained by a normal mode sampling, see *Computational details*).

Table 1. Time to traverse the transition zone and time gap of C–C bond formation for Diels–Alder reaction of diene (1,3-butadiene and 2,3-dimethyl-1,3-butadiene) and dienophile (ethene and fullerene C_{60}, respectively) at 298 K. The bond-forming time and -dissociating time are also shown with standard deviations. Medians are given in parentheses. Uncertain trajectories were removed, hence, the total number of trajectories is fewer than 1000.

Reaction	Average time to traverse the transition zone (fs)	Average bond forming time (fs)	Average bond dissociating time (fs)	Number of trajectories: reactive/total
1,3-butadiene + ethene	57.8 (55.0) ± 15.3	35.2 (31.5) ± 17.4	119.7 (117.75) ± 24.5	894/938
2,3-dimethyl-1,3-butadiene + C_{60}	84.7 (81.0) ± 22.4	43.4 (38.0) ± 39.7	268.3 (255.5) ± 97.2	841/917

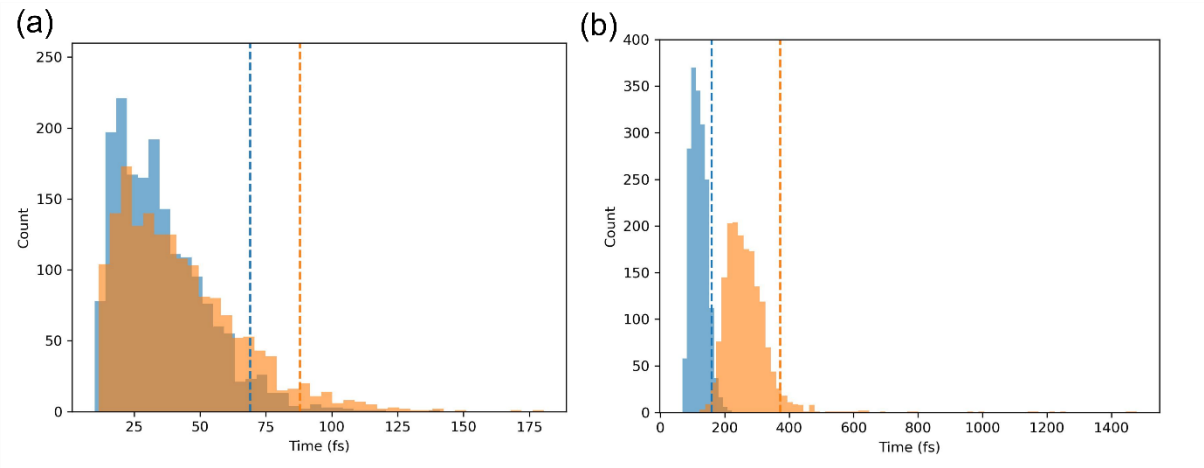

Figure 4. The histogram of the C–C a) bond-forming time and b) bond-dissociation after crossing the transition state of the Diels–Alder reaction between 1,3-butadiene and ethene (blue), and between 2,3-dimethyl-1,3-butadiene and fullerene (orange). The bonds are considered formed if they are shorter than 1.6 Å. The bonds are considered dissociated if they are longer than 5 Å for the first time. The time within which 95% of bonds are formed or dissociated is shown as the dashed line.

Hence, our dynamics simulations uncovered a pedagogically interesting situation when the kinetically faster reaction (according to simple considerations based on TS theory) takes longer to pass through the transition zone (the barrier of C_{60}+2,3-dimethyl-1,3-butadiene reaction is smaller by 7.8 kcal/mol than of ethene+1,3-butadiene, Figure 1, and, therefore, the former reaction must be faster according to TS theory). Of course, the transition state theory is only concerned with the overall reaction rate for converting reactants to products rather than with the speed of passing through the barrier. Our comparison of dynamics and static calculations clearly shows that only the dynamical calculations can capture the minute details of the barrier shape. Using only static calculations in an attempt to rationalize this dynamics behavior is not an easy task. For example, the barrier width is the first suspect to check[38] for conceptual rationalization why the bonds form and break faster after passing the TS zone, but, as mentioned before, the IRC calculations show essentially the same barrier width for both reactions and that's why cannot explain these trends. Hence, only analyzing the barrier height and width is insufficient. We need to take into account the topology near TS zone and overall barrier shape.

Apparently, the fullerene reaction involves passing through a much flatter barrier than the ethene reaction. Because the latter is more exothermic by 24.9 kcal/mol (Figure 1), it leads to the higher energy barrier measured from the products which translates to the stronger thermodynamic driving force and the higher kinetic energy of atoms moving faster away from the transition state. The transition zone (but not the barrier width as defined by IRC!) is also broader for the reaction between fullerene and 2,3-dimethyl-1,3-butadiene as the bonds to be formed range from 1.86 to 2.60 Å compared to the range of 2.02 to 2.52 Å in the reaction between ethene and 1,3-butadiene (see also the histogram of the bond lengths in the initial conditions, Figures S1, S2).

To summarize, large systems can display qualitatively different behavior due to their size and extensive dynamics simulations are essential to uncover them as we demonstrate on an example of the Diels–Alder reaction of C_{60} fullerene with 2,3-dimethyl-1,3-butadiene. These simulations are now possible with efficient active learning implementations and should become standard. Our study unveiled the crucial shape of the barrier shape and noncovalent interactions that can lead to prolonged alignment phases including complex dynamics behavior before the reaction happens.

Computational details

The MLatom ecosystem[39, 40] was used in all the simulations. UB3LYP/6-31G* calculations are done via Gaussian 16[41], the D4 dispersion correction via dftd4,[31, 42] and calculations with machine learning ANI models via TorchANI[43] interfaces to MLatom. Unrestricted B3LYP (UB3LYP) was chosen because some trajectories may potentially undergo the radical stepwise mechanism.[3] We did not observe such cases though. The $\hat{S}^2$ in the DFT calculations were all zero indicating that using UB3LYP did not lead to any spin contamination. ANI models were trained with the default MLatom settings whose settings are default ones in MLatom. The models are trained on 90% of the labeled data set and validated on the remainder.

Geometry optimization and frequency calculations are done through the interface to Gaussian[44]. The initial conditions were sampled from the harmonic quantum Boltzmann distribution[27, 45] at 298 K using the normal modes analysis of TS. In addition, the TS state of the Diels–Alder reaction of C_{60} with 2,3-dimethyl-1,3-butadiene has several low-frequency modes which can result in very distorted structures in normal mode sampling (as observed before for similar sampling procedures[44]), hence, we set these frequencies as 100 cm^{-1} if they are smaller than this value; this procedure was introduced here but later found useful also in the context of nonadiabatic dynamics submitted earlier than this work[46].

The trajectories were propagated with the time step 0.5 fs in the NVE ensemble as implemented in MLatom[47] with batch parallelization[27]. One thousand trajectories were propagated in each direction (forward and backward, where the difference is only in the initial velocities, which are set in opposite directions). The settings and detailed outcome of active learning are reported in Table S1 of SI.

In this study, we used the development version of MLatom and most of the simulations can be performed with the already-released version, while we are preparing the full release with all the remaining capabilities.

Data availability

Data is available as described in [url upon publication] (will be assigned public DOI upon publication).

Code availability

Code is available as described in [url upon publication]. All simulations can be performed with the open-source MLatom (https://github.com/dralgroup/mlatom) and MD with the trained models can be run on XACS cloud computing[48].

Author contributions

P.O.D. conceived the project. Q.Z. performed static calculations and their analysis. Y.H. and Q.Z. carried out the active learning, and performed quasi-classical dynamics. Y.H. made additional implementations for active learning and analysis. All authors analyzed the results of dynamics simulations. P.O.D. and Y.H. wrote the original version of the manuscript with input from Q.Z. All authors revised the manuscript. Y.H. and Q.Z. prepared all the figures.

Acknowledgments

P.O.D. acknowledges funding by the National Natural Science Foundation of China (No. 22003051 and funding via the Outstanding Youth Scholars (Overseas, 2021) project), the Fundamental Research Funds for the Central Universities (No. 20720210092), and via the Lab project of the State Key Laboratory of Physical Chemistry of Solid Surfaces. This project is supported by Science and Technology Projects of Innovation Laboratory for Sciences and Technologies of Energy Materials of Fujian Province (IKKEM) (No: RD2022070103).

References

(1) Wheeler, R. V.; Wood, W. L. CCXXXV.—The mechanism of thermal decomposition of the normal olefins. *J. Chem. Soc.* **1930**, *0* (0), 1819–1828. DOI: 10.1039/jr9300001819.

(2) Rowley, D.; Steiner, H. Kinetics of diene reactions at high temperatures. *Discussions of the Faraday Society* **1951**, *10*, 198–213. DOI: https://doi.org/10.1039/DF9511000198.

(3) Black, K.; Liu, P.; Xu, L.; Doubleday, C.; Houk, K. N. Dynamics, transition states, and timing of bond formation in Diels-Alder reactions. *Proc. Natl. Acad. Sci.* **2012**, *109* (32), 12860–12865. DOI: 10.1073/pnas.1209316109.

(4) Mitchell, E. C.; Scott, T. R.; Bao, J. J.; Truhlar, D. G. Application of Multiconfiguration Pair-Density Functional Theory to the Diels-Alder Reaction. *J. Phys. Chem. A* **2022**, *126* (47), 8834–8843. DOI: 10.1021/acs.jpca.2c06433.

(5) James, N. C.; Um, J. M.; Padias, A. B.; Hall, H. K., Jr.; Houk, K. N. Computational investigation of the competition between the concerted Diels-Alder reaction and formation of diradicals in reactions of acrylonitrile with nonpolar dienes. *J. Org. Chem.* **2013**, *78* (13), 6582–6592. DOI: 10.1021/jo400900x.

(6) Reveles, J. U.; Kc, G.; Baruah, T.; Zope, R. R. Diels-Alder addition to $H_2O@C_{60}$ an electronic and structural study. *Chem. Phys. Lett.* **2017**, *685*, 198–204. DOI: 10.1016/j.cplett.2017.07.062.

(7) Karimi, J.; Izadyar, M.; Nakhaeipour, A. The reactivity enhancement in Diels–Alder cycloaddition of 1,3-diene by cation encapsulation to C_{60}: a computational insight. *Struct. Chem.* **2020**, *31* (5), 1821–1829. DOI: 10.1007/s11224-020-01538-4.

(8) Bloodworth, S.; Whitby, R. J. Synthesis of endohedral fullerenes by molecular surgery. *Commun. Chem.* **2022**, *5* (1), 121. DOI: 10.1038/s42004-022-00738-9.

(9) Zhang, Y.; Cao, C.; She, Y.; Yang, Y. F.; Houk, K. N. Molecular Dynamics of Iron Porphyrin-Catalyzed C-H Hydroxylation of Ethylbenzene. *J. Am. Chem. Soc.* **2023**, *145* (26), 14446–14455. DOI: 10.1021/jacs.3c03773.

(10) Tyukina, S. P.; Velmiskina, J. A.; Dmitrienko, A. O.; Medvedev, M. G. Binomial Uncertainty in Molecular Dynamics-Based Reactions Analysis. *J. Phys. Chem. Lett.* **2024**, 2105–2110. DOI: https://doi.org/10.1021/acs.jpclett.3c03540.

(11) Unke, O. T.; Chmiela, S.; Sauceda, H. E.; Gastegger, M.; Poltavsky, I.; Schutt, K. T.; Tkatchenko, A.; Muller, K. R. Machine Learning Force Fields. *Chem. Rev.* **2021**, *121* (16), 10142–10186. DOI: 10.1021/acs.chemrev.0c01111.

(12) Meuwly, M. Machine Learning for Chemical Reactions. *Chem. Rev.* **2021**, *121* (16), 10218–10239. DOI: 10.1021/acs.chemrev.1c00033.

(13) Chmiela, S.; Vassilev-Galindo, V.; Unke, O. T.; Kabylda, A.; Sauceda, H. E.; Tkatchenko, A.; Müller, K.-R. Accurate global machine learning force fields for molecules with hundreds of atoms. *Sci. Adv.* **2023**, *9* (2), eadf0873. DOI: doi:10.1126/sciadv.adf0873.

(14) Westermayr, J.; Gastegger, M.; Voros, D.; Panzenboeck, L.; Joerg, F.; Gonzalez, L.; Marquetand, P. Deep learning study of tyrosine reveals that roaming can lead to photodamage. *Nat. Chem.* **2022**, *14* (8), 914–919. DOI: 10.1038/s41557-022-00950-z.

(15) Nandi, A.; Zhang, P.; Chen, J.; Guo, H.; Bowman, J. M. Quasiclassical simulations based on cluster models reveal vibration-facilitated roaming in the isomerization of CO adsorbed on NaCl. *Nat. Chem.* **2021**, *13* (3), 249–254. DOI: 10.1038/s41557-020-00612-y.

(16) Li, Z.; Fu, Y. L.; Luo, Z.; Yang, S.; Wu, Y.; Wu, H.; Wu, G.; Zhang, W.; Fu, B.; Yuan, K.; et al. Roaming in highly excited states: The central atom elimination of triatomic molecule decomposition. *Science* **2024**, *383* (6684), 746–750. DOI: 10.1126/science.adn3357.

(17) Upadhyay, M.; Topfer, K.; Meuwly, M. Molecular Simulation for Atmospheric Reactions: Non-Equilibrium Dynamics, Roaming, and Glycolaldehyde Formation following Photoinduced Decomposition of syn-Acetaldehyde Oxide. *J. Phys. Chem. Lett.* **2024**, *15* (1), 90–96. DOI: 10.1021/acs.jpclett.3c03131.

(18) van der Oord, C.; Sachs, M.; Kovacs, D. P.; Ortner, C.; Csanyi, G. Hyperactive learning for data-driven interatomic potentials. *NPJ Comput. Mater.* **2023**, *9* (1), 168. DOI: 10.1038/s41524-023-01104-6.

(19) Li, Z.; Kermode, J. R.; De Vita, A. Molecular dynamics with on-the-fly machine learning of quantum-mechanical forces. *Phys. Rev. Lett.* **2015**, *114* (9), 096405. DOI: 10.1103/PhysRevLett.114.096405.

(20) Jinnouchi, R.; Karsai, F.; Kresse, G. On-the-fly machine learning force field generation: Application to melting points. *Phys. Rev. B* **2019**, *100* (1), 014105. DOI: 10.1103/PhysRevB.100.014105.

(21) Kulichenko, M.; Barros, K.; Lubbers, N.; Li, Y. W.; Messerly, R.; Tretiak, S.; Smith, J. S.; Nebgen, B. Uncertainty-driven dynamics for active learning of interatomic potentials. *Nat. Comput. Sci.* **2023**, *3* (3), 230–239. DOI: 10.1038/s43588-023-00406-5.

(22) Zhang, L.; Lin, D.-Y.; Wang, H.; Car, R.; E, W. Active learning of uniformly accurate interatomic potentials for materials simulation. *Phys. Rev. Mater.* **2019**, *3* (2). DOI: 10.1103/PhysRevMaterials.3.023804.

(23) Xie, Y.; Vandermause, J.; Ramakers, S.; Protik, N. H.; Johansson, A.; Kozinsky, B. Uncertainty-aware molecular dynamics from Bayesian active learning for phase transformations and thermal transport in SiC. *npj Comput. Mater.* **2023**, *9* (1), 36. DOI: 10.1038/s41524-023-00988-8.

(24) Brezina, K.; Beck, H.; Marsalek, O. Reducing the Cost of Neural Network Potential Generation for Reactive Molecular Systems. *J. Chem. Theory Comput.* **2023**, *19* (19), 6589–6604. DOI: 10.1021/acs.jctc.3c00391.

(25) Herr, J. E.; Yao, K.; McIntyre, R.; Toth, D. W.; Parkhill, J. Metadynamics for training neural network model chemistries: A competitive assessment. *J. Chem. Phys.* **2018**, *148* (24), 241710. DOI: 10.1063/1.5020067 (acccessed 3/25/2024).

(26) Young, T. A.; Johnston-Wood, T.; Zhang, H.; Duarte, F. Reaction dynamics of Diels–Alder reactions from machine learned potentials. *Physical chemistry chemical physics : PCCP* **2022**, *24* (35), 20820–20827. DOI: https://doi.org/10.1039/D2CP02978B.

(27) Hou, Y.-F.; Zhang, L.; Zhang, Q.; Ge, F.; Dral, P. O. Physics-informed active learning for accelerating quantum chemical simulations. *arXiv:2404.11811v1 [physics.chem-ph]* **2024**.

(28) Young, T. A.; Johnston-Wood, T.; Zhang, H.; Duarte, F. Reaction dynamics of Diels-Alder reactions from machine learned potentials. *Phys. Chem. Chem. Phys.* **2022**, *24* (35), 20820–20827. DOI: 10.1039/d2cp02978b.

(29) Mukherjee, S.; Barbatti, M. A Hessian-Free Method to Prevent Zero-Point Energy Leakage in Classical Trajectories. *J. Chem. Theory Comput.* **2022**, *18* (7), 4109–4116. DOI: 10.1021/acs.jctc.2c0021.

(30) Stephens, P. J.; Devlin, F. J.; Chabalowski, C. F.; Frisch, M. J. Ab Initio Calculation of Vibrational Absorption and Circular Dichroism Spectra Using Density Functional Force Fields. *J. Phys. Chem.* **1994**, *98* (45), 11623–11627. DOI: 10.1021/j100096a001.

(31) Caldeweyher, E.; Mewes, J.-M.; Ehlert, S.; Grimme, S. Extension and evaluation of the D4 London-dispersion model for periodic systems. *Phys. Chem. Chem. Phys.* **2020**, *22* (16), 8499–8512. DOI: 10.1039/D0CP00502A.

(32) Petersson, G. A.; Bennett, A.; Tensfeldt, T. G.; Al-Laham, M. A.; Shirley, W. A.; Mantzaris, J. A complete basis set model chemistry. I. The total energies of closed-shell atoms and hydrides of the first-row elements. *J. Chem. Phys.* **1988**, *89* (4), 2193–2218. DOI: 10.1063/1.455064.

(33) Petersson, G. A.; Al-Laham, M. A. A complete basis set model chemistry. II. Open-shell systems and the total energies of the first-row atoms. *J. Chem. Phys.* **1991**, *94* (9), 6081–6090. DOI: 10.1063/1.460447.

(34) Dinadayalane, T. C.; Vijaya, R.; Smitha, A.; Sastry, G. N. Diels−Alder Reactivity of Butadiene and Cyclic Five-Membered Dienes ($(CH)_4X$, X = CH_2, SiH_2, O, NH, PH, and S) with Ethylene: A Benchmark Study. *J. Phys. Chem. A* **2002**, *106* (8), 1627–1633. DOI: 10.1021/jp013910r.

(35) Dinadayalane, T. C.; Geetha, K.; Sastry, G. N. Ab Initio and Density Functional Theory (DFT) Study on [1,5] Sigmatropic Rearrangements in Pyrroles, Phospholes, and Siloles and Their Diels−Alder Reactivities. *J. Phys. Chem. A* **2003**, *107* (28), 5479–5487. DOI: 10.1021/jp034642v.

(36) Smith, J. S.; Isayev, O.; Roitberg, A. E. ANI-1: an extensible neural network potential with DFT accuracy at force field computational cost. *Chem Sci* **2017**, *8* (4), 3192-3203. DOI: 10.1039/c6sc05720.

(37) Fukui, K. The path of chemical reactions - the IRC approach. *Acc. Chem. Res.* **1981**, *14* (12), 363–368. DOI: 10.1021/ar00072a001.

(38) Qiu, G.; Schreiner, P. R. The Intrinsic Barrier Width and Its Role in Chemical Reactivity. *ACS Cent. Sci.* **2023**, *9* (11), 2129–2137. DOI: 10.1021/acscentsci.3c00926.

(39) Dral, P. O.; Ge, F.; Hou, Y.-F.; Zheng, P.; Chen, Y.; Barbatti, M.; Isayev, O.; Wang, C.; Xue, B.-X.; Pinheiro Jr, M.; et al. MLatom 3: A Platform for Machine Learning-Enhanced Computational Chemistry Simulations and Workflows. *J. Chem. Theory Comput.* **2024**, *20* (3), 1193–1213. DOI: 10.1021/acs.jctc.3c01203.

(40) *MLatom: A Package for Atomistic Simulations with Machine Learning*; Xiamen University, Xiamen, China, http://MLatom.com, 2013–2024. (accessed 2024/05/15).

(41) *Gaussian 16 Rev. B.01*; Wallingford, CT, 2016. (accessed 2024/06/15).

(42) *DFT-D4, Version 3.5.0*; Mulliken Center for Theoretical Chemistry, University of Bonn, 2024. (accessed 2024/06/15).

(43) Gao, X.; Ramezanghorbani, F.; Isayev, O.; Smith, J. S.; Roitberg, A. E. TorchANI: A Free and Open Source PyTorch-Based Deep Learning Implementation of the ANI Neural Network Potentials. *J. Chem. Inf. Model.* **2020**, *60* (7), 3408–3415. DOI: 10.1021/acs.jcim.0c00451.

(44) Hjorth Larsen, A.; Jørgen Mortensen, J.; Blomqvist, J.; Castelli, I. E.; Christensen, R.; Dułak, M.; Friis, J.; Groves, M. N.; Hammer, B.; Hargus, C.; et al. The atomic simulation environment-a Python library for working with atoms. *J. Phys.: Condens. Matter* **2017**, *29* (27), 273002. DOI: 10.1088/1361-648X/aa680e.

(45) McQuarrie, D. A. *Statistical Thermodynamics*; University Science Books: CA, 1973.

(46) Zhang, L.; Pios, S. V.; Martyka, M.; Ge, F.; Hou, Y.-F.; Chen, Y.; Chen, L.; Jankowska, J.; Barbatti, M.; Dral, P. O. MLatom Software Ecosystem for Surface Hopping Dynamics in Python with Quantum Mechanical and Machine Learning Methods. *J. Chem. Theory Comput.* **2024**. DOI: 10.1021/acs.jctc.4c00468.

(47) Zhang, L.; Hou, Y.-F.; Ge, F.; Dral, P. O. Energy-conserving molecular dynamics is not energy conserving. *Phys. Chem. Chem. Phys.* **2023**, *25* (35), 23467–23476. DOI: https://doi.org/10.1039/D3CP03515H.

(48) *Xiamen Atomistic Computing Suite (XACS), https://XACScloud.com*; Xiamen University: 2022-2024. (accessed 2024/06/15).